Chapter 4

Experimental set-up

In this chapter we discuss the experimental configurations and the measurements of the statistical moments that were performed in different flow configurations such as: grid turbulence, jet turbulence and cylinder wake turbulence. The experiments for cylinder wake were done in a wind tunnel, and the jet and grid turbulence experiments were performed in a water channel. The velocity measurement were obtained by means of hot-wire anemometry and a sonic velocimeter SONTEK-3D. A description of the experimental set-ups, the hot-wire, the sonic velocimeter and the flow configurations are presented here.

4.1 Hot-wire anemometer

The hot-wire anemometer is one of the best instrument so far developed for the measurements and analysis of the micro structure of the velocity of a streaming gas or liquid. The high frequency resolution of the hot wire sensor cannot be matched by any other anemometers except for Doppler laser systems. Also, it can be made small enough and fast enough to measure within the dissipation range. The sensitive element of the anemometer is a thin wire suspended between two prongs.

The hot wire sensors are made from certified materials selected to maintain consistent properties. The wire most commonly used is platinum-coated tungsten. Tungsten wires have a high temperature coefficient of resistance which is an important property in obtaining good signals. A platinum coating provides oxidation resistance, which improves the long term stability of the sensor.

The mechanical strength of a hot-wire is sufficiently high for applications in gases at rather high velocities, and in non-conducting liquids at medium velocities. Figure 4.1 shows probe type configurations of various DISA standard hot-wire probes.

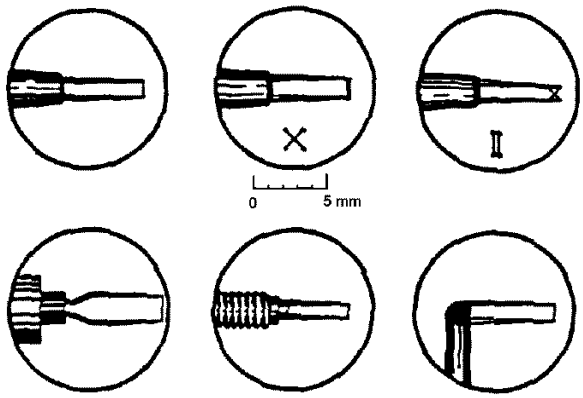

Figure 4.1: Hot-wire configurations.

4.2 Velocity response

The use of a hot sensing element for measurements of particle velocity in fluid flows relies on laws governing convective transfer. These laws are generally too complicated to permit a theoretical calculation of the relation between the flow velocity and the heat flux from a probe, and the relation must therefore be found experimentally, using similarity laws. Moreover, heat will be transfered both by natural convection and by conduction to the wire support or film-backing material.

The operating principale is that the probe has initially the same temperature T_f as the flow and has an electrical resistance R_f. When the probe is heated to temperature T_w, the resulting resistance R_w will then be given by

$$R_w = R_f[1 + c_T(T_w - T_f)], \tag{4.1}$$

where c_T is the temperature coefficient of the probe. For thermal equilibrium, the rate of heat loss $c_h S(T_w - T_f)$ from the probe, where c_h is the heat transfer coefficient and S is the surface area of the wire probe, must be equal to the heating power I^2R generated by the electric current I. Therefore, the calibration curve for flow

perpendicular to the probe is written as

$$\frac{I^2 R_w}{R_w - R_f} = A + BU^n, \tag{4.2}$$

where U is the local flow velocity, often $n = 1/2$ is used, A and B are determined experimentally and verified over the desired range of speeds. For constant temperature operation $R_w/(R_w - R_f)$ is also taken as constant and equation (4.2) can be simplified as:

$$I^2 = A' + B'U^{1/2}. \tag{4.3}$$

Equations (4.2) and (4.3) are called King's law. Of course, a hot-wire has finite length and the convective end losses must be taken into account. Therefore, in practice the precise relation between $I(R_w)$ and U is determined in a calibration procedure that uses a laminar flow with known steady velocity, U.

4.3 Determination of fluctuating components

Calibration of the hot-wire is usually done in wind-tunnel with low-intensity turbulence that could be called a static calibration; the same calibration is generally also used to obtain the velocity fluctuations. Equations for the fluctuating quantities are given by Hinze (1959), Champagne and Sleicher (1967), and Larsen and Busch (1974). Typical sensor configurations are: a single sensor (perpendicular to the flow), an X-configuration, and a three-dimensional system.

4.3.1 Single sensor

The sensor used for measuring turbulence must be parallel to the z axis and flow in the x, y plane with x is the mean flow coordinate. The situation is illustrated in figure 4.2. We can write

$$U = [(\bar{u} + u')^2 + v'^2 + kw'^2]^{1/2}, \tag{4.4}$$

where u', v' and w' are the flow fluctuations components, $\bar{u}$ is the mean flow velocity. Such a sensor is first-order sensitive only to the mean flow and to the fluctuations u'; the lateral component v' enters only as a second-order correction.

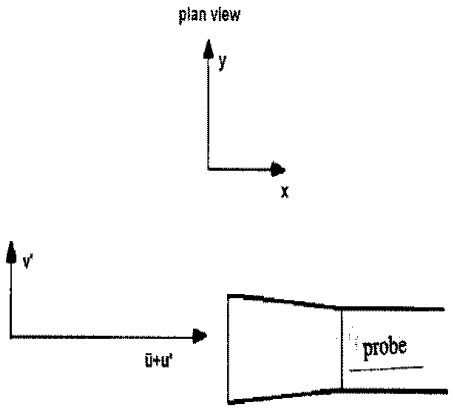

Figure 4.2: Hot-wire configuration to measure the longitudinal velocity component.

4.3.2 X-configuration

For the X-configuration we may consider the flow in a natural coordinate system. If the X-sensor forms an angle of 45^o with $\bar{u}$ it will be equally sensitive to the two fluctuating velocity components in the plan formed by $\bar{u}$ and the wire axis. Thus, two wires placed at an angle of 45 with respect to the mean velocity will generate the following AC output signals (figure 4.3):

$$\begin{aligned} V_I &= s_I(u - v), \\ V_{II} &= s_{II}(u + v). \end{aligned} \tag{4.5}$$

If the sensitivities of the two anemometers are adjusted so that $s_I = s_{II} = s$ the sum and the difference of the two signals are:

$$\begin{aligned} V_I + V_{II} &= 2su \\ V_{II} - V_I &= 2sv. \end{aligned} \tag{4.6}$$

That is, the two fluctuating velocity components u and v can be determined in a simple and direct manner from the X-sensor. The vertical velocity w can be determined in a similar manner after having rotated the sensor 90 degrees.

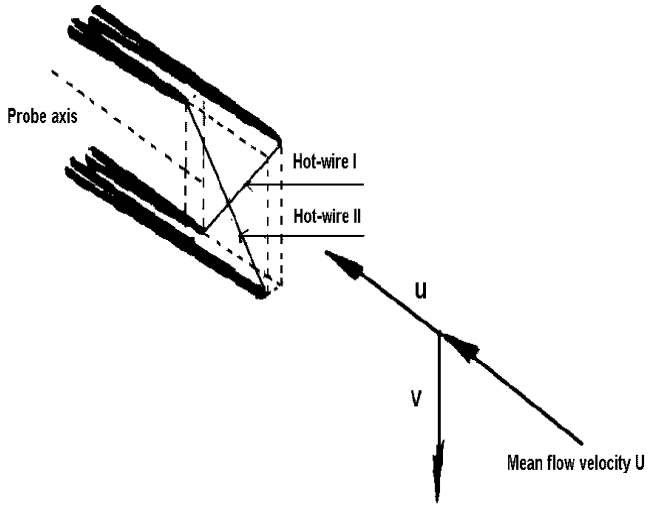

Figure 4.3: X-probe used for measurements of transverse velocity components.

4.4 Constant-temperature anemometry

Two different basic circuits are available for the measurement of turbulent velocities: constant-current anemometry (CCA) and constant-temperature anemometry (CTA), of which the first is the older. In CCA the electric current I is kept constant and the temperature of the sensor (and hence its electric resistance) changes due to fluctuating cooling caused by the fluctuating velocity. In CTA the most rapid velocity fluctuations can be measured without the use of complex compensation circuitry. This is more demanding.

In our measurement of velocity fluctuations, we use only CTA. The idea behind this method is to minimize the effect of the probe terminal inertia by keeping the sensitive element at a constant temperature (resistance) and using the heating current as a measure of heat transfer and hence velocity. The constant-temperature principal of operation was first proposed by Kennelly in 1909. However, this requires a sophisticated and well designed electronic system. In figure 4.4 the electrical circuit of anemometer is schematically shown. The Wheatstone-bridge consists of two fixed resistors R_1 and R_s, the hot-wire probe resistance R_w and a variable resistor R_v.

The bridge is in exact balance at a certain voltage supplied by the servo amplifier. A slight change of the probe resistance, due to a change in the convective cooling of the sensor, will produce a small unbalance the voltage. This voltage, after having amplification, is used to adjust the bridge voltage (probe current) in such a way that the bridge will be kept close to balance.

The values of the resistors R_1, R_s and R_v determine the resistance of the probe for which the bridge is in equilibrium. The working temperature (resistance) of the probe, R_w, is determined by

$$\frac{R_w}{R_s} = \frac{R_1}{R_v}. \tag{4.7}$$

The CTA anemometer is more sensitive at higher working temperature. The voltage Vout is a measure of the velocity u of the flow.

Another advantage of a constant-temperature system is that a higher overheat may be used without the risk of burning out the probe; the higher overheat reduces the temperature sensitivity of the hot sensor relative to its flow sensitivity. Typical hot-wire overheat for a constant-current system is 60^{o}C, while for a constant temperature system it is 200^{o}C at a wind speed of 5 m/s.

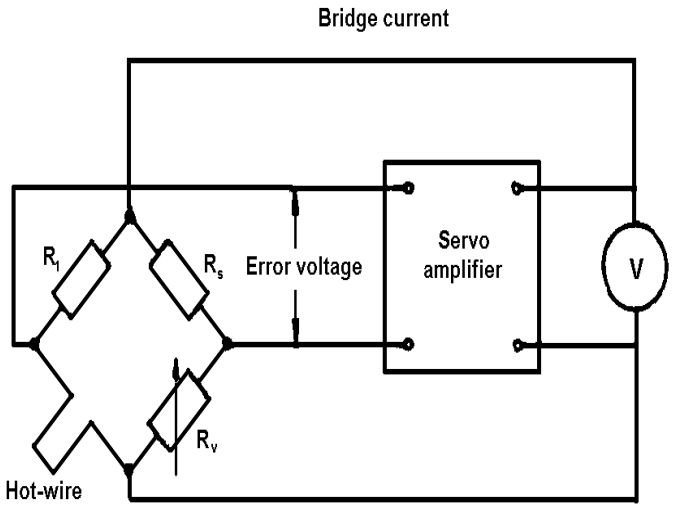

Figure 4.4: Constant-temperature anemometer.

4.5 Calibration of probe

Evaluation of flow velocity components from probes using equation (4.3) depends on the sensor configuration being very close to the assumed geometry. However, the relation between the flow velocity $\bar{u} + u'$ and the output voltage Vout of the anemometer can not be fully determined on a theoretical basis. The probes are usually calibrated in a laminar flow.

Before each measurement, the probes were calibrated in our experiments using portable automated calibration equipment, (Wojciechowski (1998)). The static calibration of the detectors including their filters, amplifiers, ADCs, etc was done. In this way, the probes were not moved after the calibration and possible deviations of the instrumentation were included in the calibration.

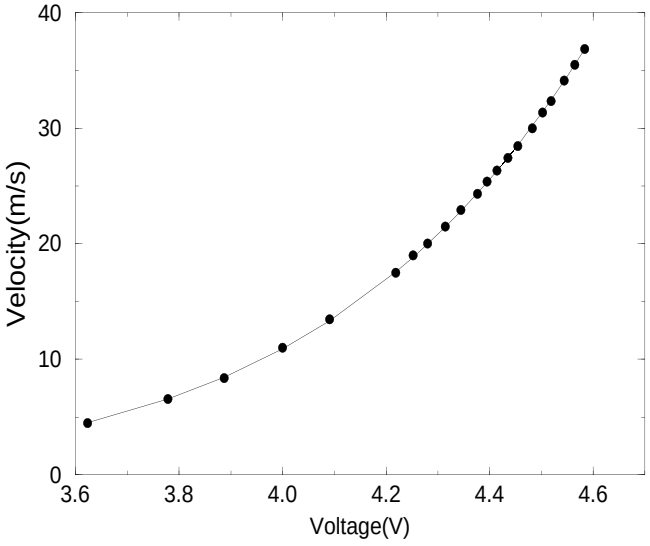

Figure 4.5: Typical calibration curve.

The probe was calibrated by generating a known laminar flow perpendicular to the probe. The measured velocities from this calibrations were given as:

$$U(V) = c_0 + c_1 V + c_2 V^2 + c_3 V^3 + c_4 V^4, \tag{4.8}$$

where c_0,.., c_4 are the fit parameters. This equation was used to generate the calibration tables for use in our real-line data processing. Moreover, calibration of the hot wire sensor at low velocities poses problems because of the generally insufficient sensitivity of conventional calibration standards, such as Pitot-static tubes. Therefore,

we used velocities of more than 0.5 m/s in order to avoid significant error. Figure 4.5 shows an example of a measured and fitted calibration curve for a hot-wire probe.

4.6 Measurement and data processing

As was mentioned above, the hot-wire probe was used to measure the velocity fluctuations in a closed wind tunnel. The hot-wire was made of platinum-plated tungsten and a constant temperature anemometer (DISA55M10) was used. The hot-wire was 1 mm long and its diameter was 2.2 μm. Figure 4.6 shows schematically the hot-wire probe used. The probe was positioned at different locations in the tunnel. Velocity values stored on a magnetic tape were digitized using a 12 bit analog to digital converter and processed on a digital computer.

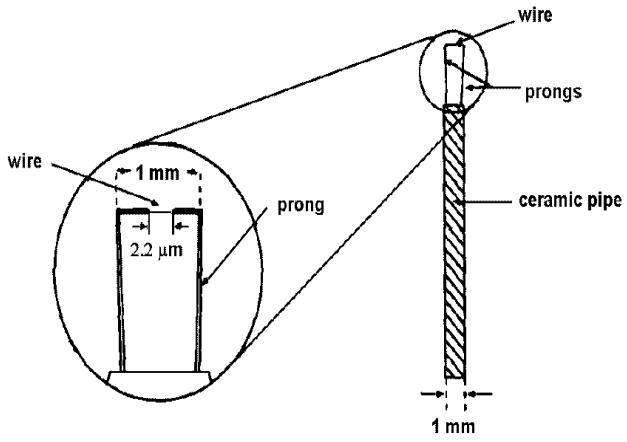

Figure 4.6: Schematic views of the hot-wire probe used in the longitudinal measurements.

In order to reduce the noise level, the signal was filtered with a cut off frequency of 16 KHz. The sampling frequency was f_s=50 KHz. 2.10^6 samples were acquired in order to study with high accuracy the statistical behavior. The turbulence intensity $(\bar{u^2})^{1/2}/U$ was lower than 0.4 in all the experiments, therefore, Taylor's hypothesis

(Taylor (1938)) was used; it was assumed that

$$\ell = x^{(2)} - x^{(1)} = U\tau, \tag{4.9}$$

where τ is the temporal increments. The question of how the Taylor hypothesis should be corrected when the turbulence intensity is higher is addressed by Lumley (1965) and Pinton & Labbe (1994).

4.7 Acoustic Doppler Velocimeter (ADV)

The Acoustic Doppler Velocimeter (ADV) shown in figure 4.7 is a versatile, high-precision instrument that measures all three flow velocity components. The measurements are insensitive to water quality which allows for a wide range of applications. The ADV uses acoustic sensing techniques to measure flow in a remote sampling volume. ADVs are used in laboratories, wave basins, rivers, estuaries and oceanographic research.

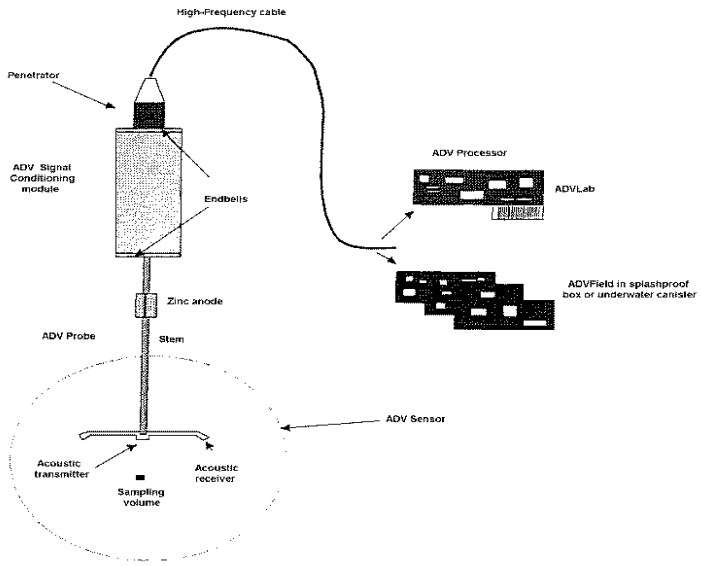

Figure 4.7: Naming conventions for the Acoustic Doppler Velocimeter (ADV).

4.7.1 Doppler principle

The ADV is based on the Doppler principle to measure flow in a remote sampling volume. First, a short acoustic pulse of known frequency is transmitted along the vertical axis. The echo from the water is received in three small transducer elements, amplified in the conditioning module and digitized/analyzed in the processing board. The frequency shift between the pulse and the received echo is proportional to the water velocity.

To ensure proper operation, the echo must be strong enough to allow a proper calculation of the frequency shift. If the echo is weak, the calculation will be statistically noisy and the velocity data will show significant errors and short-term variability.

4.7.2 Signal-to-Noise Ratio (SNR)

The strength of the echo is measured in terms of a signal-to-noise ratio (SNR) expressed in dB and displayed for each receiving beam together with the velocity data at the computer display. When collecting raw data at sampling frequency 25 Hz, a SNR that is consistently above 15 dB is recommended. The scattering strength is determined by the concentration and size of the particles suspended in the water. The particles can be naturally occurring suspended sediments (rivers, ocean, sand-filled or polluted model basins), bubbles entrained from pump systems (this is often the case in high velocity flumes), or artificial (seeding). If the SNR remains low even after seeding, it is important to clean the receiving and transmitting transducers by gently rubbing the emissions surface. This will clean off residues or bubbles that may have collected and are blocking the sound.

4.7.3 Seeding and distance from sampling volume to boundary

The concentration of scattering micro particles in water may be important in order to avoid the velocity data noise. The noise can also be remedied by adding seeding material or injecting bubbles. However, before each experiment we cleaned the water flume and we added custom-made spherical nylon particles with a density close to that of water and a size of around 10 μm. The choice of this size is motivated by the relatively strong echo that these particles generate per unit of concentration. Smaller particles, for example 1 μm, used to seed Laser Doppler systems, were not used because the required concentration is high.

The center of the sampling volume is positioned approximately 5 cm or 10 cm below the transit transducer located at the center of the probe. The distance to the boundary is measured by echo-sounding, and can be shown on the computer display. The measurement corresponds to the distance from the middle of the sampling volume to the nearest boundary. The sampling volume is of finite extent and the minimum distance to the boundary that still permits data collection is 4-6 mm for a standard set-up. Some experimentation is required because the exact limit depends both on the condition of the boundary and on the software configuration. The effective sampling volume is about 20 mm^3.

4.7.4 Ordinate system and calibration

The ADV sensor consists of one transmitting transducer and three receiver arms. The red receiver arm on the 3D down-looking probe should point in the direction of the mean flow (the x-axis) and the value for the velocity along this axis (figure 4.8). The directions of the y-axis and the z-axis are based on the definition of a right-handed coordinate system where z is pointing upwards (towards the conditioning module). The same convection is followed for upward-looking systems, i.e. positive z is toward the conditioning module.

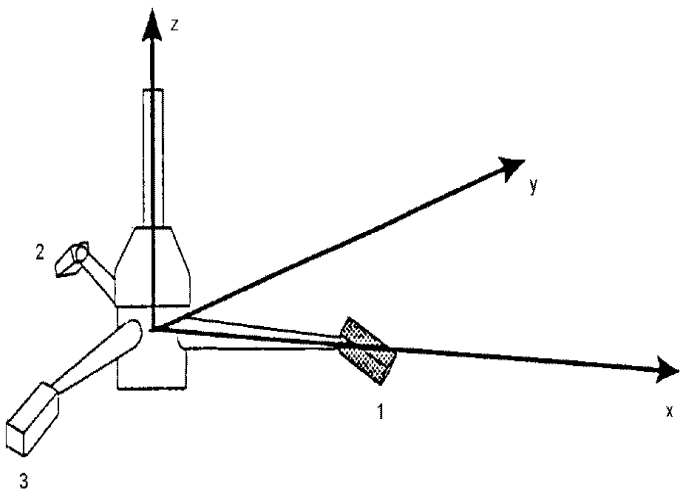

Figure 4.8: Standard 3D down-looking probe.

ADV calibration factors are determined by the speed of sound and by the angles between the transmitter and receiving arms. To ensure that the correct speed of sound is used in the water, temperature and salinity must be entered in the data acquisition software. The calibration angles are measured at the factory and need only be changed when a new probe is installed. The measurements unit used in the water flume measurements was a SONTEK-3D velocimeter.

4.8 Characteristic parameters of the flows investigated

For each experiment the characteristic quantities of the turbulent flow were calculated from the longitudinal time series. The mean velocity U is,

$$U = \langle u(t) \rangle_t, \tag{4.10}$$

the root-mean-square velocity σ_u,

$$\sigma_u = \langle (u(t) - U)^2 \rangle_t^{1/2}, \tag{4.11}$$

thus the turbulence intensity is calculated as

$$I_t = \frac{\sigma_u}{U}. \tag{4.12}$$

The local isotropy was assumed in order to calculate the mean energy dissipation $\langle \epsilon \rangle$,

$$\langle \epsilon \rangle = 15 \nu U^{-2} \left\langle \left(\frac{du}{dt} \right)^2 \right\rangle_t. \tag{4.13}$$

The Kolmogorov length scale η is

$$\eta = (\nu^3 / \langle \epsilon \rangle)^{1/4}, \tag{4.14}$$

hence, the Taylor micro scale is defined as

$$\lambda = \sigma_u U \left\langle \left(\frac{du}{dt} \right)^2 \right\rangle_t^{-1/2}. \tag{4.15}$$

This scale was used to define the local Reynolds number

$$R_\lambda = \frac{\sigma_u \lambda}{\nu}. \tag{4.16}$$

The correlation function is given after applying Taylor's hypothesis as

$$R(l) = \frac{\langle u(x)u(x+l)\rangle}{\sigma_u^2}, \tag{4.17}$$

and from the spatial correlation function we obtain the integral length scale L

$$L = \int_0^\infty R(l)dl. \tag{4.18}$$

4.9 Flow configurations

In this section we describe the three types of flow configuration investigated in this thesis, jet, grid and cylinder wake turbulence. Two tunnels were used. The first is a wind tunnel and with a closed working section, which was used to generate cylinder turbulence. The wind tunnel was 2 m long with square cross-section 0.3 $\times$ 0.3 cm^2 and can generate a flow with a maximum speed of 50 m/s (figure 4.9). The measurements of the turbulent flow were obtained by means of a CTA hot-wire sensor. The wind tunnel experiments were performed at the Aeronautical Laboratory of the Warsaw University of Technology under the supervision of Dr. Jan Wojciechowski by Eric Gaudin and O. Ben Mahjoub.

The second experimental set up was an open water channel, which was used to generate both jet and grid turbulence. The water channel had a test section with a length of 1.5 m, base cross-section 0.15 m and height 0.3 m (figure 4.10). The measurements were mostly obtained by means of the SONTEK-3D velocimeter, and the maximum velocity flow that could be generated was 3 m/s. The water channel experiments were performed at the Fluid Dynamics Laboratory at the U.P.C during 1997-1999.

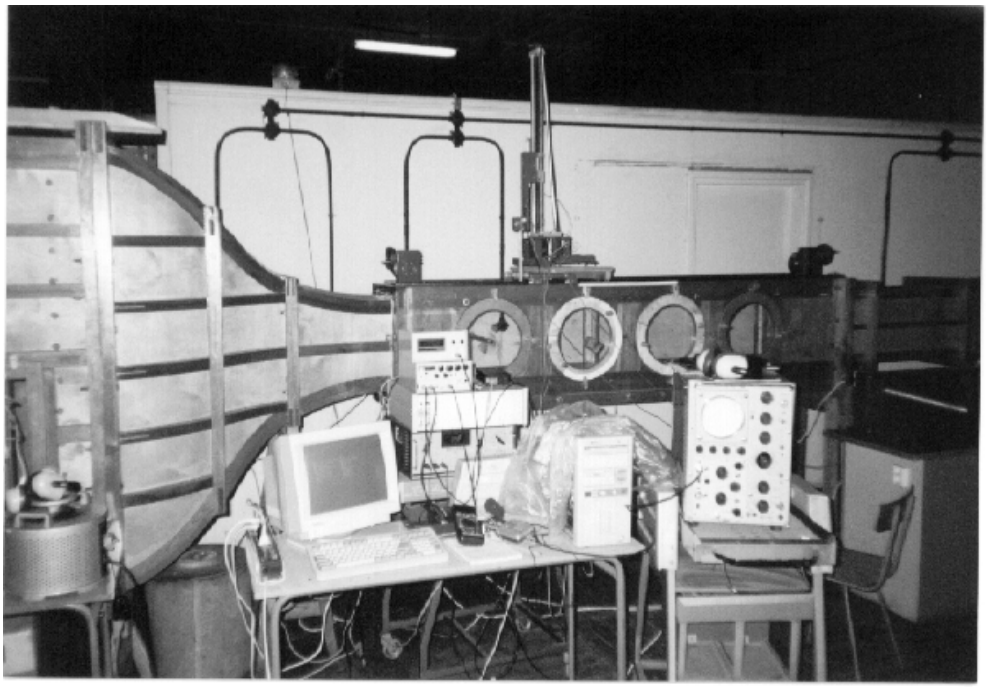

Figure 4.9: Experimental set-up of cylinder wake turbulence at the University of Warsaw.

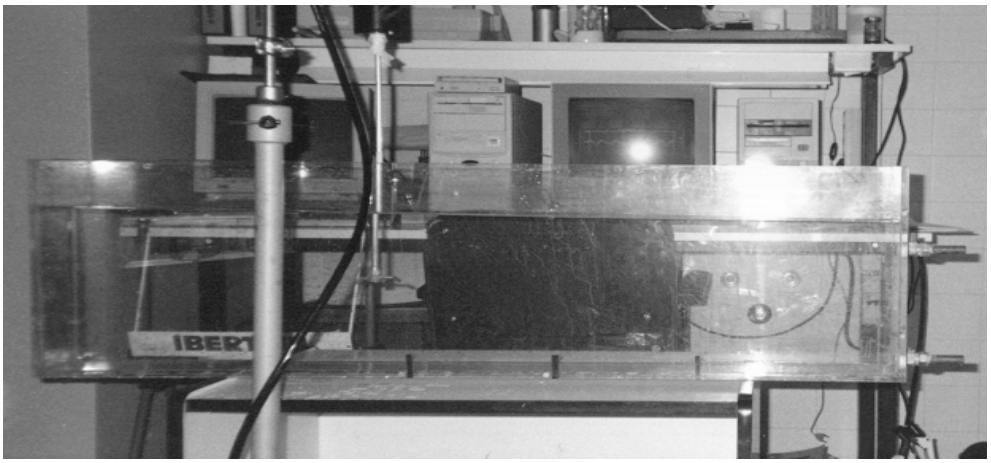

Figure 4.10: Experimental set-up of grid and jet turbulence at Universitat Politecnica de Catalunya.

4.9.1 Grid turbulence

Turbulence is generated by a grid placed in the flow generated in the recirculating water flume. The flow field downstream of the grid can be divided into three regions. The first is the developing region nearest the grid where the rod wakes are merging, the flow is non-homogeneous and non-isotropic and, consequently, there is production of turbulent kinetic energy. This region is followed by one where the flow is nearly homogeneous and locally isotropic but where there is important energy transfer from one scale to another. This is a region of the decay power-law. The third region comprises the final period of decay where viscous effects act directly on the large energy-containing scales at the furthest location downstream from the grid.

The turbulent flow downstream of the grid is described in detail by Monin & Yaglom (1975), Champagne *et al.* (1970), Comte-Bellot & Corrsin (1971) and Mohamed & La Rue (1990). Grant & Nisbit (1957) found that the non-homogeneity and non-isotropy of the flow decreases very slowly with the downstream distance from the grid and that the position where the flow becomes homogeneous and isotropic depends on the mesh size of the grid M and the Reynolds number Re_M. Mohamed & La Rue (1990) used the skewness of the velocity $S(u) = \langle u^3 \rangle / \langle u^2 \rangle^{3/2}$ to study the isotropy of the flow and found that the skewness factor approaches a constant value, depending on Re_λ for $x/M > 25$ where x is the distance from the grid. In addition, they found that the value of the decay exponent is 1.3 with a root mean square variation of 0.024, and this value does not depend on the initial conditions.

The structure functions measured in grid-turbulence have been studied by Benzi *et al.* (1993) and Baudet *et al.* (1993) for different Reynolds numbers Re_λ. Camussi *et al.* (1996) have measured longitudinal and transversal structure functions in low Reynolds numbers (Re_λ=2.5, 6, 12.5, 20, 36) using an X-wire probe.

In this thesis the grid turbulence measurements were performed in the open water tunnel described in the previous section. The channel is operated in a closed return mode and has a measured free-stream turbulence intensity of less than 0.4 % in the velocity range 5-20 m/s. The turbulence generator was one grid constructed of polished aluminum bars. The bar diameter was 0.5 cm with corresponding mesh size of 3 cm. The grid has a solidity ratio of 0.34 and is placed 0.5 m and 0.2 m downstream of the exit of the contraction of the water channel. The measurements have were recorded by the SONTEK-3D velocimeter. The sampling frequency was 25 Hz and number of samples taken on each run was 10^5.

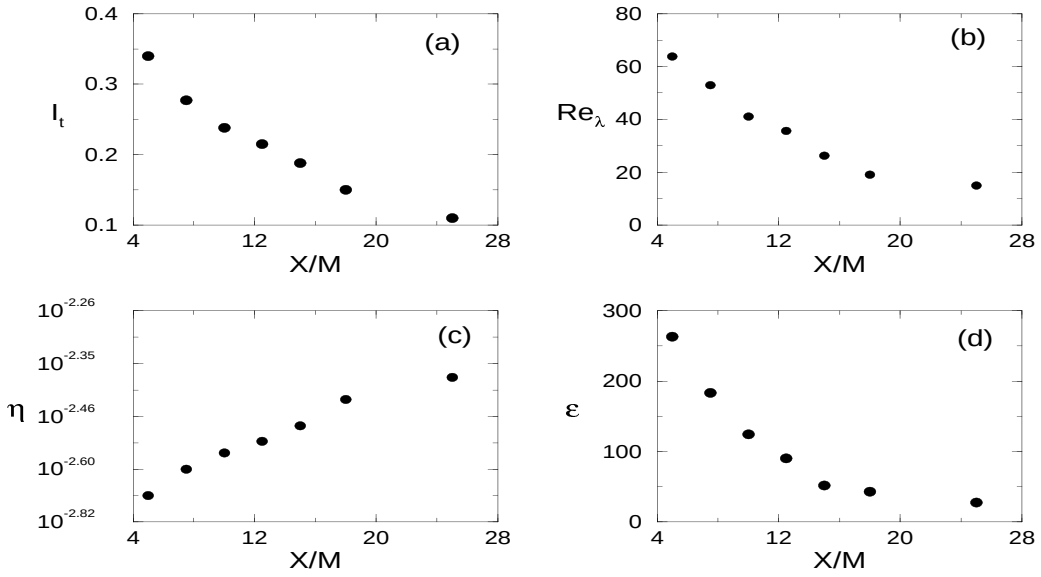

Figure 4.11: Evolution of turbulence intensity I_t (a), Reynolds number Re_λ (b), Kolmogorov's scale η (c) and energy dissipation ϵ (d) as a function of the downstream distance X/M for grid turbulence.

As mentioned above the grid turbulence intensity was found to be lower than 0.35 at all locations in the flow. We could therefore use Taylor's hypothesis. Figure 4.11 show the distribution of the turbulence intensity I_t, Reynolds number Re_λ, Kolmogorov's scale η and energy dissipation ϵ as function of the downstream distance from the grid.

4.9.2 Cylinder wake turbulence

The flow past an axisymmetric body thus departs from irrotational theory not only around the body but also behind it. The latter region of rotational flow is called the wake. However, the structure of the wake behind a body depends on the particular body. In the particular case of a circular cylinder wake, many studies have been reported, due to the simplicity in setting up such an arrangement in an experimental or computational laboratory. Townsed (1948), Ubervoi & Freymuth (1969) and Champagne (1978) studied the turbulent flow behind cylinders; they found that at a downstream distance $x/D > 90$, where D is the diameter of the cylinder, the flow does not depend on the initial conditions.

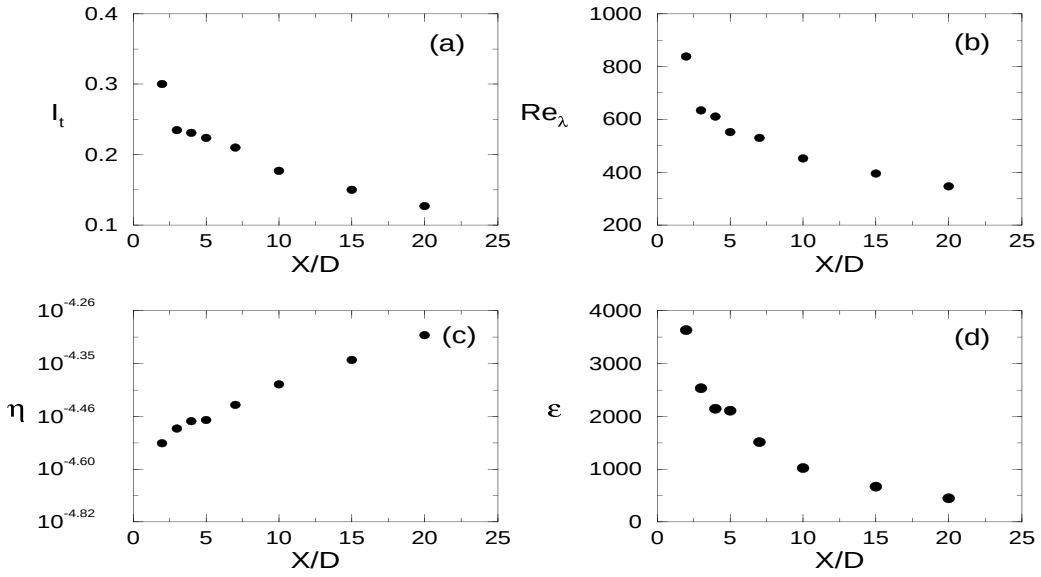

Figure 4.12: Evolution of turbulence intensity I_t (a), Reynolds number Re_λ (b), Kolmogorov's scale η (c) and energy dissipation ϵ (d) as a function of the downstream distance X/D for cylinder wake turbulence at the lateral distance $Y/D = 0$.

A great many measurements of the velocity structure functions have been carried out for the cylinder wake for different Reynolds numbers Re_λ. Baudet *et al.* (1993) and Benzi *et al.* (1993) measured the structure functions for the Reynolds numbers (Re_λ= 225, 342, 475) using two cylinder diameter of 5 and 10 cm. Meneveau & Sreenivasan (1991) and Thoroddsen & van Atta (1992) measured small-scale structure of turbulence in cylinder wake at distances $x/D = 90$ and $x/D = 58$.

In our measurements performed by Gaudin at the University of Warsaw, the cylinder wake was generated by a cylinder of 1 cm in diameter. The cylinder was placed along the wind tunnel axis at 15 cm behind the exit contraction. The measurements were recorded at various locations in the flow by a CTA hot-wire anemometer with sampling frequency of 50 KHz. The use of Taylor's hypothesis was also justified in the cylinder wake because the maximum turbulence level was about 30% as shown in figure 4.12. The evolution of the high Reynolds number Re_λ, Kolmogorov's scale η and energy dissipation ϵ as a function of the downstream distance X/D for cylinder wake turbulence at the lateral distance $Y/D = 0$ is also shown in the figure. In most locations, high turbulence intensity was measured only at $X/D = 2$, indicating the complex structure of the wake and the influence of the coherent structures.

4.9.3 Jet turbulence

Jet turbulence is one of the most interesting flows, and it has been the subject of intensive experimental investigation for many years (Wygnanski & Fiedler (1969), Antonia *et al.* (1986) and Panchapakesan & Lumley (1993)). It is used to illustrate the presence of eddy motion at all scales. A jet is produced when fluid is ejected from an orifice. Because of their simplicity, the geometries that have been most investigated are a circular orifice giving an axisymmetric jet and a long thin slit giving a two-dimensional jet. Close behind the orifice the layer has zero width, and this layer increases as a function of distance from the orifice.

At the jet-axis the velocity remains constant at the distance $x \leq x_d$, x_d is the downstream distance where the shear layers coincide and cover the entire jet. For distance $x \geq x_d$, the velocity decreases with the downstream distance from the nozzle and the flow become independent on the initial conditions, as showed by Hinze (1987).

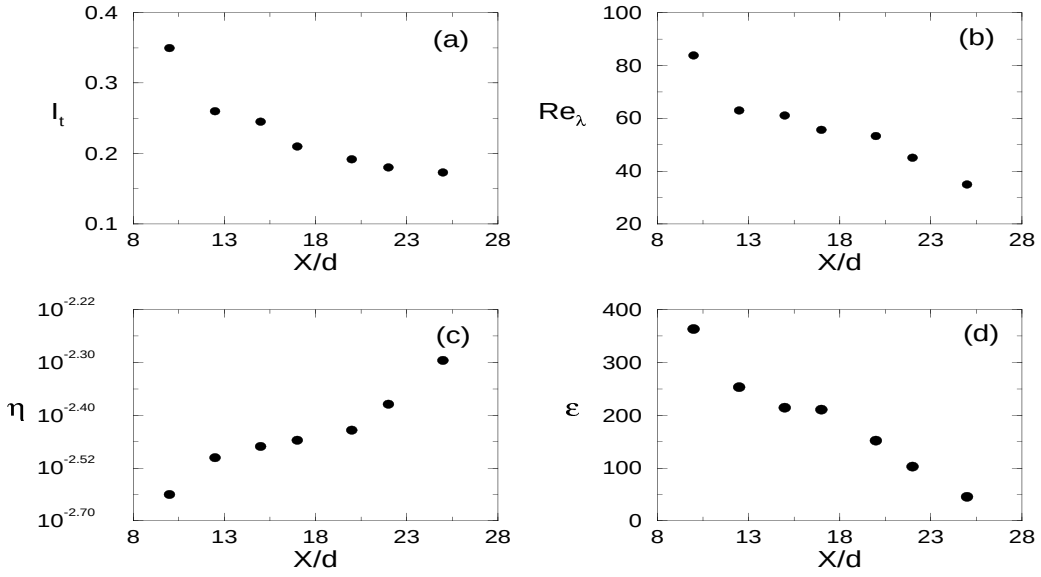

Figure 4.13: Evolution of turbulence intensity I_t (a), Reynolds number Re_λ (b), Kolmogorov's scale η (c) and energy dissipation ϵ (d) as a function of the downstream distance X/d for jet turbulence.

Antonia *et al.* (1982), Anselmet *et al.* (1984) and Castaing *et al.* (1990), measured structure functions and velocity difference distribution functions in different jet flows. In this thesis the jet turbulence was created by a circular jet in the open water

channel. The jet nozzle diameter d was 2 cm. The velocity was recorded at different locations in the flow by the SONTEK-3D velocimeter. Most of the measurements were done near the jet nozzle, where the flow is strongly non-homogeneous and non-isotropic, because of the interest of studying the scaling laws of non-homogeneous and non-isotropic turbulence, which play an important role in the understanding of the turbulent dynamics in non-homogeneous geophysical flows both in the ocean and in the atmosphere.

Evolution of turbulence intensity I_t, Reynolds number Re_λ, Kolmogorov's scale η and energy dissipation ϵ as a function of downstream distance X/d from jet nozzle are shown in figure 4.13. As can be seen the turbulence intensity in our jet experiment was less than 30 % everywhere, also favoring the use of Taylor's hypothesis, which is used in all the structure function measurements reported in this thesis.